Interpretation of Spatially Decaying Ion-Acoustic Waves

J. L. HIRSHFIELD, J. H. JACOB, AND D. E. BALDWIN
Mason Laboratory, Yale University, New Haven, Connecticut 06520
(Received 17 June 1969; final manuscript received 18 June 1970)

Detailed examination is given to circumstances surrounding the excitation and detection of spatially propagating ion-acoustic disturbances in a plasma. For relatively weak damping, a theory is presented to show the major influence on spatial signal evolution engendered by source coupling details, by source geometry, and by three-dimensional ion trajectories. In particular, near-zone and far-zone regions are identified for a disk source. Fresnel interference can dominate the near zone (within which many experiments are performed), so that serious questions can be raised as to the interpretation of observed decays. For relatively strong decays, the transition to the ballistic, three-dimensional, free-streaming solution is presented. Experiments are presented to illustrate some features of the theory, including measurements of Landau damping with $0.04 < k_i/k_r < 0.2$ for $0.6 < \omega/\omega_{pi} < 1.4$. Observed Fresnel interference patterns are compared with theory.

I. INTRODUCTION

Amongst the several active areas of study of linearized waves in equilibrium plasmas, considerable recent attention has been devoted to ion-acoustic waves. The last few years have seen activity in both theory and experiment and interplay between the two is now underway. Early measurements concentrated on tests of the predicted phase velocity of the waves, particularly for bounded plasma.[1] More recently, measurements of wave decay have been reported[2] together with interpretations in terms of Landau damping. A thoery applicable to experiments on spatial decay has been developed by Gould,[3] who solved for the spatial evolution of an ion-acoustic wave propagating in space away from a transparent oscillating dipole exciting grid. Gould's theory was based on a modeling of the conditions under which the Q machine experiments of Wong, Motley, and D'Angelo[4] had previously been carried out. In his analysis of this experiment, Gould pointed out that the earlier dispersion-relation theory of Fried and Gould,[5] valid for the time-dependent decay problem, was suspect for the steady-state problem. Later experiments by Wong[6] showed discrepancies with Gould's theory, and Wong suggested that the contribution of the source electrons assumed in the theory may not have corresponded to the experimental conditions. Since Wong's measured decay was *weaker* than that calculated by Gould, it is difficult to see how electron collisions (neglected in the theory) could explain the discrepancy, a postulate advanced by Wong. It was suggested by Wong, however, that the details of the interaction at the wave source could well influence the observed decay.

Further experiments on Q machines include those of Sato *et al.*[7] who extended the frequency range to above the ion plasma frequency, and Andersen *et al.*[8] who were able to increase the electron-to-ion temperature ratio from 1 to 3 and thus observed decreased damping.

In dc discharges, numerous experiments have been carried out by Alexeff and co-workers.[9] They found good agreement between experiment and the elementary theoretical value of the phase velocity $(kT_e/M_i)^{1/2}$, and observed remarkable decreases in signal amplitude upon introduction of a minority concentration of light ions, whose thermal velocity was comparable to the phase velocity. Although Alexeff *et al.* observed strong signal decrease as the frequency exceeded $0.7\omega_{pi}$, careful damping measurements were not quoted. Sessler[10] reported a wave response for $\omega > \omega_{pi}$, as well as for $\omega < \omega_{pi}$, but with damping which was not a particularly dramatic function of ω/ω_{pi}, a contrast to the usual theory. Differences between the observations and Gould's theoretical model have been discussed by Sessler and Pearson.[11]

In a general critique of the effects of the phase-mixed electron–ballistic contribution to a spatially decaying response, we[12] concluded that observed damping rates with ratios of imaginary-to-real wave-number k_i/k_r not much less than 0.4 were subject to an interpretation which did not depend at all upon the collective plasma feature. While the thrust of the arguments in Ref. 12 was directed at the high-frequency response of a plasma ($\omega \simeq \omega_{pe}$), we suggested there that similar considerations applied at low frequencies ($\omega < \omega_{pi}$). We shall demonstrate this point rigorously later in the present paper. The criterion mentioned above would then exclude the Q machine measurements with $T_e = T_i$ from unequivocal interpretation.

The main object of the present paper is to point out effects which can enter measurements of signal decay under conditions typical of some laboratory

studies. These effects depend upon the details of the coupling between the source (say a grid, or grids) and the plasma, upon the finite geometry of the source, and upon the three-dimensional motions of the plasma particles. The combined result of these several effects is a predicted decay response which is not exponential and not necessarily monotone. However if the damping is not too weak, a prescription is given for fitting a simple exponential to the observed decay, with results in fair agreement with the one-dimensional theory.

The points raised here suggest that a careful examination is needed of the interpretation given to nonlinear observations such as nonlinear Landau damping[13] or ion-wave echoes,[14] if it should turn out that conditions for excitation of linear disturbances are not clear in these studies. These latter observations have been both carried out using Q machines with strong magnetic fields, and the present paper only considers magnetic field free plasma. It might be expected, however, that the three-dimensional effects to be discussed would still be important for the ions unless the ion gyroradius r_g were much smaller than the source dimension; and that the source coupling details would be ill-understood unless the ion gyroradius were less than the electron Debye length, and thus ion trajectories near grid elements would be calculable. For cesium ions at 2500°K, $r_g \simeq 540/B$ cm, where B is the magnetic field strength in gauss. Thus the first constraint requires $B \gtrsim 5$ kG for a 1 cm source disk. The second condition requires $B \gtrsim 54$ kG for a plasma density of 10^9 cm^{-3}.

Experiments are presented in this paper which demonstrate some of the points evident in the analysis. When the collisional damping is large (at a pressure of 4 mTorr in argon), the value of k_i is obtained by assuming simple exponential decay. Theoretical motivation for such a procedure is presented. At lower background pressures the Fresnel-like interference is more pronounced, and is compared in detail with theory.

This paper is organized with the experimental configuration chosen to demonstrate the interactions discussed in Sec. II; this then hopefully motivates the theoretical exposition of Sec. III; the experimental results are discussed in Sec. IV.

II. EXPERIMENTAL SET-UP

The physical requirements for a steady-state plasma in which to study ion-acoustic wave propagation and decay include: low background gas pressure (< 10 mTorr) to minimize ion–atom collisions; low electron and ion densities ($< 10^{10}$ cm^{-3}) to minimize electron–ion and ion–ion collisions, and to provide a large Debye length; significant ratio $T_e/T_i (> 3)$ so as to avoid strong wave damping due to the ions; reasonable spatial homogeneity ($< 5\%$) over the plasma volume (~ 100 cm^3) in which the waves propagate; and low noise fluctuation ($< 1\%$ rms ion saturation current to a small Langmuir probe) so as to allow detection of weak signals, and so as to avoid overestimates of damping due to time averaging of phase-varying signals (when lock-in detection is used).

These requirements were met by employing the discharge-tube configuration shown in Fig. 1. The Pyrex discharge bottle itself is roughly cylindrical,

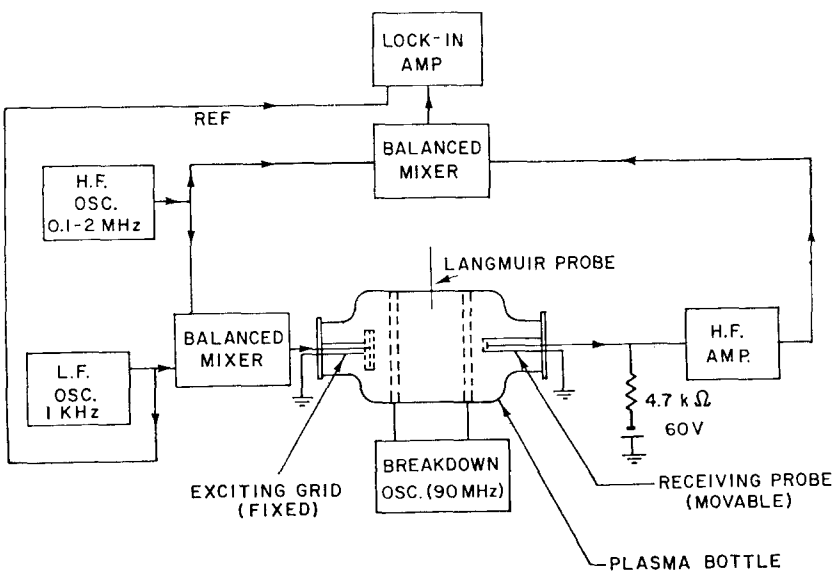

FIG. 1. Block diagram of experimental apparatus.

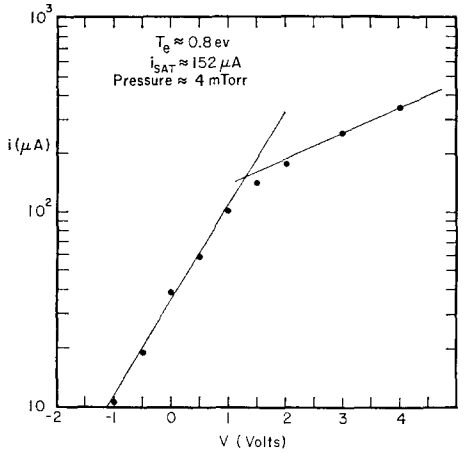

FIG. 2. Langmuir probe curve. Probe current vs voltage.

with diameter 20 cm and length 33 cm. Copper straps 1 cm wide encircle the bottle at symmetrical positions 13 cm apart. These straps are connected via sliding taps to the coil in a tank circuit of a 10 W 90 MHz oscillator. The data to be presented were all taken with argon as the filling gas at a pressure of 3–4 mTorr. A movable cylindrical Langmuir probe (diameter 7.5×10^{-2} cm, length 0.5 cm) was used to measure electron density and temperature, and a typical probe characteristic is shown in Fig. 2. The inferred electron temperature is 0.80 eV. All data to be presented are for an electron density of 5×10^8 cm^{-3}, corresponding to an ion plasma frequency of 740 KHz.

Under these conditions, the Debye shielding length λ_D is 3×10^{-2} cm. This large Debye length made it possible to construct a wave transducer whose influence upon the particle trajectories was approximately calculable. Three or four fine mesh circular grids of diameter 4.5 cm were positioned parallel to one another at an intergrid spacing of 7.5×10^{-2} cm, about two Debye lengths.[15] The grid mesh spacing was 2.5×10^{-2} cm, less than one Debye length. The two outer grids were connected together and, with the supporting structure, provided the dc reference potential for the plasma. The inner grid was connected to the external rf generator by coaxial transmission line. The plasma potential was about 6 V positive with respect to ground, so that plasma electrons were virtually all turned around in a retarding sheath external to the structure. Ions, on the other hand, were accelerated in this sheath and traveled through the grid structure nearly parallel to the axis. Approximately 50% of the incident ions were transmitted through the structure, due to the fractional transmission of each grid. The ion space charge in the intergrid spaces perturbed the constant vacuum electric field by a negligible amount.[16]

This three-grid transducer was positioned axially in the discharge tube, and served as the wave transmitter. The wave receiver was constructed as a grid-shielded ion collector. The grid (at ground potential) reflected electrons, while the ions were accelerated to the collector. The receiver diameter was 0.205 cm, and could be moved axially in the discharge over an excursion of 5 cm. As long as the distance between transmitter and receiver exceeded 0.5 cm, motion of the receiver did not significantly alter the plasma properties.

III. THEORY

The ingredients of a theory applicable to the experimental configuration described above should include proper source specifications and boundary conditions in a thorough three-dimensional kinetic description. While a one-dimensional fluid model for ion-acoustic wave excitation has recently been published,[17] and while the one-dimensional kinetic description of Gould[3] has received wide attention, we believe that the models chosen for analysis by these authors are too restrictive for most experiments.

For the present theory, we shall assume that the charged particle dynamics are governed by a collisionless Boltzmann equation for each species, electrons and singly charged ions. (Collisions will be included through a simple relaxation model further along.) The electric field is assumed to be curl free and is broken into three parts: $\mathbf{E}_0(\mathbf{r}, t)$, the rf field applied within the grids (and zero elsewhere); $\mathbf{E}(\mathbf{r}, t)$, the rf self-consistent field; and $\mathbf{E}_{dc}(\mathbf{r})$, the dc bias of the grids. As has been discussed above only ions experience the applied field $\mathbf{E}_0$, since in the intergrid region electrons are imagined to be excluded by the static bias $\mathbf{E}_{dc}(\mathbf{r})$. The equations are linearized so that the particle velocity distribution functions contain a small perturbed part $f_\alpha(\mathbf{v}, \mathbf{r}, t)$ relative to the unperturbed part $F_\alpha(v)$, where subscript α designates the species.

Therefore, for electrons and ions we have the kinetic equations

$$\frac{\partial}{\partial t} f_e(\mathbf{v}, \mathbf{r}, t) + \mathbf{v} \cdot \nabla f_e(\mathbf{v}, \mathbf{r}, t) - \frac{e}{m} \mathbf{E}_{dc}(r) \cdot \nabla f_e(\mathbf{v}, \mathbf{r}, t)$$

$$- \frac{e}{m} \mathbf{E}(\mathbf{r}, t) \cdot \nabla_v F_e(\mathbf{v}, \mathbf{r}) = 0; \qquad (1)$$

$$\frac{\partial}{\partial t} f_i(\mathbf{v}, \mathbf{r}, t) + \mathbf{v}\cdot\nabla f_i(\mathbf{v}, \mathbf{r}, t) + \frac{e}{M}\mathbf{E}_{dc}(\mathbf{r})\cdot\nabla f_i(\mathbf{v}, \mathbf{r}, t)$$

$$+ \frac{e}{M}[\mathbf{E}(\mathbf{r}, t) + \mathbf{E}_0(\mathbf{r}, t)]\cdot\nabla_v F_i(\mathbf{v}, \mathbf{r}) = 0; \quad (2)$$

and for the perturbed charge density $\rho(\mathbf{r}, t)$ we have Poisson's equation

$$\rho(\mathbf{r}, t) = \frac{1}{4\pi}\nabla\cdot\mathbf{E}(\mathbf{r}, t)$$

$$= e\int d^3v\,[f_i(\mathbf{v}, \mathbf{r}, t) - f_e(\mathbf{v}, \mathbf{r}, t)]. \quad (3)$$

In order to solve Eqs. (1)–(3), we must justify the replacement of the nonuniform plasma near the source by a physically equivalent uniform plasma. Both the grid separations and the dc sheath scale lengths are of the order of the electron Debye length, which is short compared with other lengths of interest. (For the ion-acoustic wavelength and the distance traveled by an electron in a period, this is certainly true. For the distance traveled by an ion in a period, this is only marginally true and contributes one of the uncertainties in this and similar work.) We approximate the true situation, and scale the grid separation to zero, allowing all electrons to be reflected by a plane barrier (sheath) of zero thickness. The ions are taken to pass through this barrier in zero time but to receive in impulse due to the field $\mathbf{E}_0$, which, of course, depends upon the time spent in the intergrid region.

In the characteristic integration of Eqs. (1) and (2), therefore, the unperturbed trajectories of the ions are taken as straight lines which may pass through the grid region. The unperturbed trajectories of the electrons are straight except when they are broken at the grid, corresponding to specular reflection. In general such considerations hold without special symmetry of $\mathbf{E}_0$. Because not all kernals of the equation are of the difference form, integral equations thus obtained are not amenable to solution by Fourier transforms. However, in the special case where $\mathbf{E}_{dc}$ and $\mathbf{E}_0$ are antisymmetric in z (the coordinate normal to the plane of the grids), $\mathbf{E}$ will likewise be antisymmetric, and the electrons which are reflected by the grids may be considered to have passed through them, meaning that all trajectories may be taken as straight lines. The contribution to the charge density when the fields are antisymmetric can be shown[18] to be the same in the two cases. The net result is that the integral equation describing the field may then be solved by Fourier transformation in space.[19] These were key considerations in the choice of transmitting grid described in the previous section.

For any function $g(\mathbf{r})$ the space transformed function is introduced via a Fourier transform

$$g(\mathbf{k}) = \int_{-\infty}^{+\infty} d^3r\, g(\mathbf{r}) \exp(+i\mathbf{k}\cdot\mathbf{r})$$

so that

$$g(\mathbf{r}) = \frac{1}{(2\pi)^3}\int_{-\infty}^{+\infty} d^3k\, g(\mathbf{k}) \exp(-i\mathbf{k}\cdot\mathbf{r}).$$

We also introduce a Laplace transform

$$g(\omega) = \int_0^{\infty} dt\, g(t) \exp(-i\omega t), \ \mathrm{Im}\,\omega < 0,$$

$$g(t) = \frac{1}{2\pi}\int_{-\infty-i\beta}^{+\infty-i\beta} d\omega\, g(\omega) \exp(+i\omega t).$$

Then, carrying out the transforms on Eqs. (1)–(3), the steady-state solution for the perturbed charge density is

$$\rho(\mathbf{k}, \omega) = \frac{i(e^2/M)\mathbf{E}_0(\mathbf{k}, \omega)\cdot\int[d^3v\nabla_v F_i/(\omega - \mathbf{k}\cdot\mathbf{v})]}{1 - (4\pi e^2/k^2M)\int d^3v\,[\mathbf{k}\cdot\nabla_v F_i/(\omega - \mathbf{k}\cdot\mathbf{v})] - (4\pi e^2/k^2m)\int d^3v\,[\mathbf{k}\cdot\nabla_v F_e/(\omega - \mathbf{k}\cdot\mathbf{v})]} \equiv \frac{\rho_{fs}(\mathbf{k}, \omega)}{D(\mathbf{k}, \omega)}, \quad (4)$$

where the denominator $D(\mathbf{k}, \omega)$ is the plasma dielectric function, which depends only upon the modulus of $\mathbf{k}$ for isotropic distributions $F_e(v)$ and $F_i(v)$, and where $\rho_{fs}(\mathbf{k}, \omega)$ is the free-streaming ion perturbation. The transform of the perturbed potential may also be obtained as $\phi(\mathbf{k}, \omega) = 4\pi\rho(\mathbf{k}, \omega)/k^2$.

We will first solve for $\rho_{fs}(\mathbf{k}, \omega)$, the numerator in Eq. (4), which is the Fourier–Laplace transform of the ion free-streaming charge density. If ions passed through the source grids into a plasma-free half-space, and if the ion density were low enough so that mutual Coulomb encounters were of minor importance, $\rho_{fs}(\mathbf{k}, \omega)$ would be the transform of the charge density in the half-space. For the actual problem at hand, where the source ions stream into a neutralizing plasma with collective Coulomb forces, $\rho_{fs}(\mathbf{k}, \omega)/D(\mathbf{k}, \omega)$ is the transformed charge density, where the $D^{-1}(k, \omega)$ brings in the plasma response (i.e., electron shielding, wavelike response, etc.).

For the three-grid transducer, under conditions discussed above where electrons are excluded and where the ion shielding length is large compared

with the intergrid spacing, the source electric field is well approximated by its vacuum value. We shall first deal with the intergrid potential: $\phi_0(z, r) = (1 - |z|/L) \cos \omega t$ for $0 < r < a$, $-L < z < L$; and $\phi_0(z, r) = 0$ elsewhere; z and r are the axial and radial coordinates of a cylindrical system centered at the (circular) grid. Thus,

$$\phi_0(\mathbf{k}) = 8\pi\phi_0 \frac{a}{L} \frac{1}{(k_z^2 k_\perp)} \sin^2\left(\frac{k_z L}{2}\right) J_1(k_\perp a) \cos \omega t \qquad (5)$$

and $\mathbf{E}_0(\mathbf{k}) = -i\mathbf{k}\phi_0(\mathbf{k})$, since $\nabla \times \mathbf{E}_0(\mathbf{r}) = 0$. We therefore find, if we neglect the change in velocity of the ions as they pass through the dc sheaths,

$$\rho_{fs}(\mathbf{k}, \omega) = -\frac{ie^2}{M} E_0 \frac{8\pi a}{k_z^2 k_\perp} \sin^2\left(\frac{k_z L}{2}\right) J_1(k_\perp a) \cdot \int d^3v \frac{\mathbf{k}\cdot\nabla_v F_i(v)}{\omega - \mathbf{k}\cdot\mathbf{v}}, \qquad (6)$$

where $E_0 = \phi_0/L$. The velocity integral in Eq. (6) is the same as that appearing in $D(\mathbf{k}, \omega)$. [See Eq. (4).] For a Maxwellian ion distribution it is, in fact, $N(2v_i^2)^{-1} Z'(\omega/kv_i)$, where N is the ion density, v_i is the ion thermal speed, and where $Z'(\zeta)$ is the derivative of the plasma dispersion function.[20] Later, we shall find it convenient to write this integral as proportional to $[D_e(\mathbf{k}, \omega) - D(\mathbf{k}, \omega)]$, where $D_e(\mathbf{k}, \omega)$ is $D(\mathbf{k}, \omega)$ with $M \to \infty$, i.e., the "electron" dispersion function. Thus, the ion-acoustic disturbance in front of the source grid is

$$\rho(\mathbf{r}, \omega) = \frac{i}{2\pi^3} E_0 a \int d^3k \exp(-i\mathbf{k}\cdot\mathbf{r}) \frac{k^2}{k_z^2 k_\perp} \cdot \sin^2\left(\frac{k_z L}{2}\right) J_1(k_\perp a) \left(\frac{D_e(\mathbf{k}, \omega) - D(\mathbf{k}, \omega)}{D(\mathbf{k}, \omega)}\right) \qquad (7)$$

or

$$\phi(\mathbf{r}, \omega) = \frac{2i}{\pi^2} E_0 a \int d^3k \exp(-i\mathbf{k}\cdot\mathbf{r}) \frac{1}{k_z^2 k_\perp} \cdot \sin^2\left(\frac{k_z L}{2}\right) J_1(k_\perp a) \left(\frac{D_e(\mathbf{k}, \omega) - D(\mathbf{k}, \omega)}{D(\mathbf{k}, \omega)}\right). \qquad (8)$$

Let us consider the limits of strong and weak damping separately in performing the transform inversion in Eqs. (7) and (8). First, for strong damping when $\omega \ll \omega_{pi}$ and $T_e \simeq T_i$ (conditions typical for ion-acoustic studies in Q machine plasmas), the quantity $(D_e - D)/D$ is of order unity and varies gently with k. The unity in this ratio gives back $\rho_0(\mathbf{r}, \omega)$ and $\phi_0(\mathbf{r}, \omega)$, the charge and potential at the grids, while the D_e/D gives the plasma response. Since D_e/D (shown plotted versus real values of kv_i/ω for $T_e = T_i$ and $\omega = \omega_{pi}/10$ in Fig. 3) does not vary appreciably with k, one does not expect the resulting plasma disturbance to vary much from the free-streaming behavior. This is best shown explicitly by considering the ion current $\mathbf{j}_i(\mathbf{k}, \omega)$, the transform of which quantity is actually detected in many experiments. From Eqs. (2) and (4), and using the longitudinal property of the disturbance, i.e., $\mathbf{k} \times \mathbf{E} = 0$, we find we can write

$$\mathbf{j}_i(\mathbf{k}, \omega) = \mathbf{j}_{fs}(\mathbf{k}, \omega)\left(1 + \frac{D_e(\mathbf{k}, \omega) - D(\mathbf{k}, \omega)}{D(\mathbf{k}, \omega)}\right) \qquad (9)$$

where

$$\mathbf{j}_{fs}(\mathbf{k}, \omega) = -\frac{ie^2}{M} \int d^3v \mathbf{v} \frac{\mathbf{E}_0(\mathbf{k})\cdot\nabla_v F_i(v)}{\omega - \mathbf{k}\cdot\mathbf{v}}$$

is the free-streaming ion current. The first unity in Eq. (9) comes from $\mathbf{E}_0$ (the applied field), the second factor from $\mathbf{E}$ (the self-consistent field) which provides the plasma response. For equal electron and ion temperatures, where $(D_e - D)/D$ is much less than one (see Fig. 3), one sees directly that the transform of the ion current is very nearly all free streaming.

For the source model considered by Gould,[3] where the oscillating dipole sheet perturbed both electrons and ions, the $D_e(\mathbf{k}, \omega)$ in Eq. (9) is replaced by unity. Now, since $|D(\mathbf{k}, \omega)| \gg 1$ for $T_e \simeq T_i$, $|\mathbf{j}_i(\mathbf{k}, \omega)| \ll |\mathbf{j}_{fs}(\mathbf{k}, \omega)|$. The spatial variation of $\mathbf{j}_i(\mathbf{r}, \omega)$ is very nearly free streaming, however, since $D(\mathbf{k}, \omega)$ shows very little structure along the real k axis (for $T_e = T_i$). The large reduction in amplitude from the free-streaming value comes about because of the poor matching to an ion-acoustic wave of a source with even spatial E-field symmetry which drives electrons out of phase with ions.

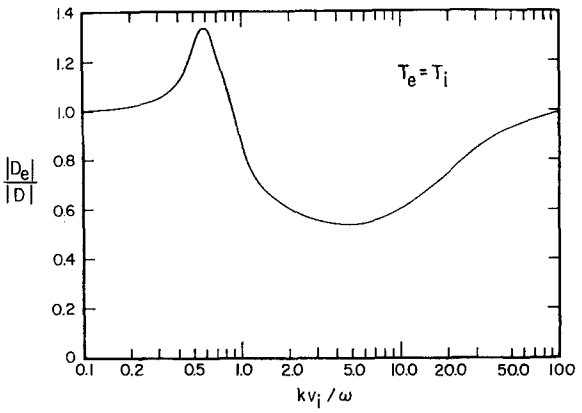

FIG. 3. Plot of $|D_e|/|D|$ vs kv_i/ω for $T_e = T_i$ and $\omega = \omega_{pi}/10$. One notes that $|D_e|/|D|$ is a smoothly varying function of kv_i/ω having a maximum of about 1.3 and a minimum of about 0.5. Thus, the ion current to a negatively biased detector is essentially the free-streaming value.

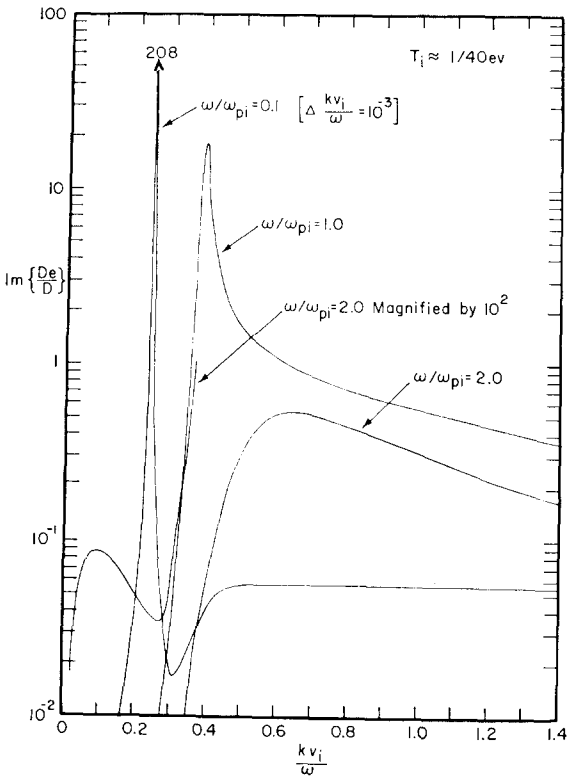

FIG. 4. Plot of $\mathrm{Im}(D_e/D)$ vs kv_i/ω for various values of ω/ω_{pi}. For $\omega/\omega_{pi} < 1$, $\mathrm{Im}(D_e/D)$ is sharply peaked about $k_r v_i/\omega = 1$ where k_r is the dominant root of $\mathrm{Re}[D(k, \omega)] = 0$. For $\omega/\omega_{pi} > 1$ the sharp peak disappears and one sees the appearance of a second weak bump at low kv_i/ω. ($T_e = 32T_i$ for these examples.)

For weak damping, $T_e \gg T_i$ and $\omega < \omega_{pi}$, $D_e(\mathbf{k}, \omega)/D(\mathbf{k}, \omega)$ is a sharply peaked function of k. This is shown in Fig. 4 for $T_e/T_i = 32$ and for several values of ω/ω_{pi}. We exploit this sharply peaked nature to derive the self-consistent electric field in the plasma given by (see Appendix A)

$$E_z(r, z, \omega) = -\frac{E_0 a L^2}{2\pi}\left[\frac{D_e(k_0)}{(\partial D/\partial k)_{k_0}}\right]k_0 \cdot \int_0^\infty dk_\perp\, J_0(k_\perp r) J_1(k_\perp a) \exp\left[iz(k_0^2 - k_\perp^2)^{1/2}\right], \quad (10)$$

where k_0 is the (complex) value of k for which $D(k, \omega) = 0$.

First, we consider the solution on the z axis, where $r = 0$. The integral in Eq. (12) can then be evaluated in closed form,[21] yielding

$$E_z(r = 0, z, \omega) = \frac{E_0 a L^2}{4\pi} k_0^4 \lambda_D^2 \frac{\omega_{pi}^2}{\omega^2} \cdot \left(\frac{z}{a}\frac{\exp\left[-ik_0(z^2 + a^2)^{1/2}\right]}{(z^2 + a^2)^{1/2}} - \frac{1}{a}\exp(-ik_0 z)\right), \quad (11)$$

where the approximate form $D(k, \omega) = 1 - (\omega_{pi}^2/\omega^2) + (1/k^2\lambda_D^2)$ has been used in evaluating $\partial D/\partial k$.

Equation (11) predicts a potential pattern similar to that found in acoustics and optics. The signal at a field point z is the result of phase interference from elementary signals propagating along rays connecting each point on the source with the field point z. Within the "near zone," given by $0 < z \lesssim \mathrm{Re}\, k_0 a^2/\pi$, strong Fresnel interference is in evidence; while in the "far zone" $z \gtrsim \mathrm{Re}\, k_0 a^2/\pi$, the potential is a monotone decaying function of z. The asymptotic behavior for $z \gg a$ is

$$E_z(r = 0, z) \approx \exp(-ik_0 z)\left(\frac{ik_0 a^2}{z} + \frac{a^2}{z^2} + \cdots\right).$$

For typical experimental conditions in this and in other work, one finds most measurements to be made in the near zone.

Numerical examples of the ion-acoustic disturbances as a function of z are shown in Figs. 5(a), (b), and (c). In these examples we have plotted the z component of the electric field [Eq. (11)] or current j for $r = 0$, since in the experiment a shielded biased electrode collects ion current which is proportional to E_z. Results at fixed frequency for several damping lengths (due to collisions) are shown in Fig. 5(a), while results for fixed damping length at several frequencies are shown in Fig. 5(b). In Fig. 5(c) we have plotted Re E_z (or Re j_z) for three different values of ω/ω_{pi} at a fixed value of k_i. Damping is included in the nondispersive regime by permitting k_0 to have a small imaginary part $k_0 \rightarrow \mathrm{Re}\, k_0(1 + i\nu_c/\omega)$ where ν_c is the ion–atom collision frequency, assuming a weakly ionized gas, taken to be argon for the examples. From the numerical examples two features of the field pattern become evident: The Fresnel interference becomes more pronounced as z increases, and as the frequency increases; and the number of Fresnel zones increases with frequency. Comparing Figs. 5(b) and (c) we see that the inclusion of the phase information [see Fig. 5(c)] de-emphasizes the interference pattern. The two dashed lines in Fig. 5(a) are the simple exponential decays for the one-dimensional case for values of $k_i \approx 1.076$ cm^{-1} and 0.269 cm^{-1}. The three-dimensional solution oscillates about the one-dimensional decay. In fact, for the case of stronger damping, k_i can be estimated with reasonable accuracy by force fitting the decay to a straight line. This procedure was followed in analyzing the data in the following section.

For the special case of equal size receiving and transmitting disks, the average value of $j_z(r, z, \omega)$

over the receiving disk is, from Eq. (10), proportional to

$$\int_0^\infty dk_\perp \, J_1^2(ka) \exp\left[iz(k_0^2 - k_\perp^2)^{1/2}\right].$$

This function has been evaluated numerically and is plotted in Fig. 6 for Im $k_0 = 0$ and for Im $k_0 =$ 0.042 cm^{-1}, the value associated with the principle Landau pole in a collisionless plasma with $T_e = 16T_i$ and $\omega = 0.27\omega_{pi}$. While the interference pattern is well-nigh obliterated, the monotone decay of such functions is not well approximated by Im k_0, unless this value be greater than about 0.5 cm^{-1}, corresponding to strong collisional damping.

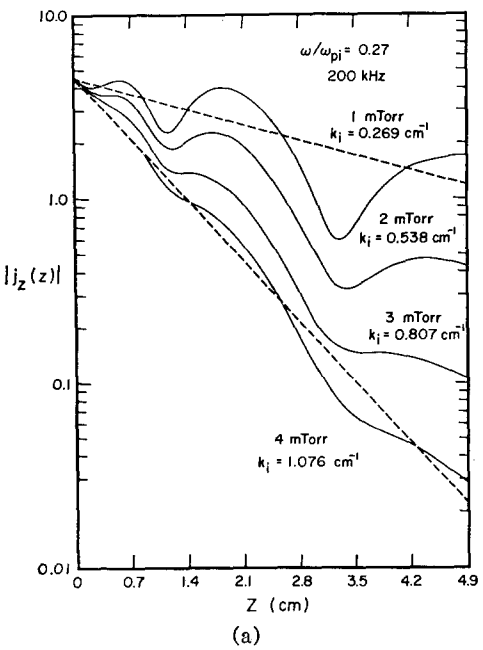

(a)

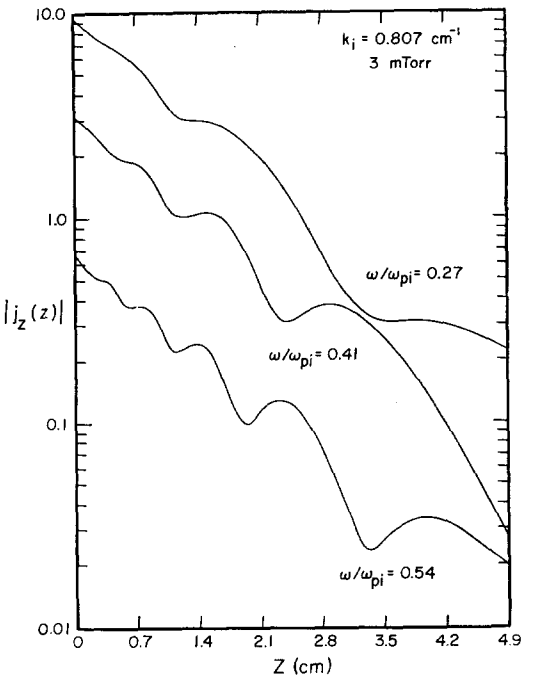

(b)

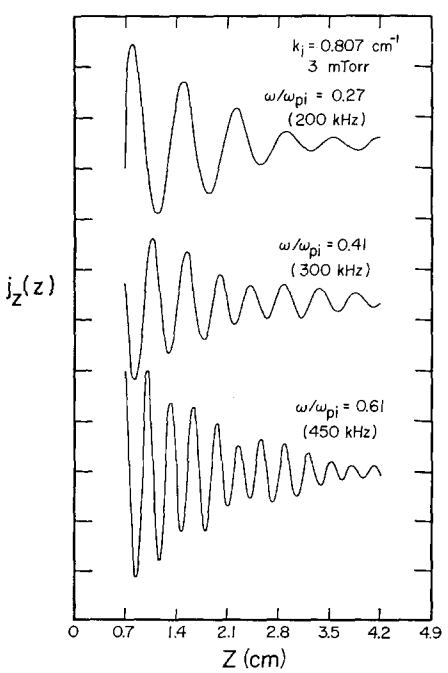

(c)

FIG. 5. (a) A theoretical semilog plot of $|j(z, r, = 0)|$ vs z. ω/ω_{pi} is fixed at 0.27 while Im k (corresponding to collisional damping) is varied. The accelerating dc sheath surrounding the transducer is neglected. (b) Same as Fig. 5(a) except for Im k fixed at 0.538 cm^{-1} (corresponding to collisional damping at an argon background pressure of 2 mTorr). ω/ω_{pi} is varied. (c) Same as Fig. 5(b) except that the phase information is included.

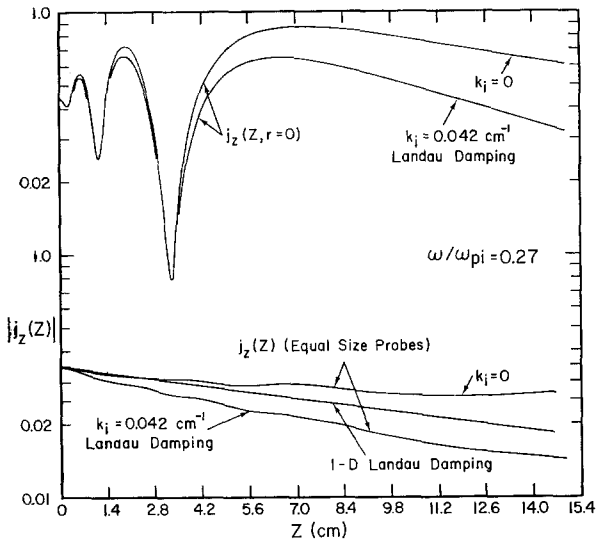

FIG. 6. The top two traces are theoretical plots of $j_z(z, r = 0)$ vs z with $\omega/\omega_{pi} = 0.27$ for Im $k = 0$ and Im $k = 0.042$ cm^{-1}. The latter value of Im k corresponds to Landau damping when $T_e = 16\ T_i$. The lower traces are theoretical plots of $j_z(z, r)$ averaged over a receiver having the same diameter as the transmitter. Notice the Fresnel-like interference pattern in the near field is no longer present. For the case of Im $k = 0$ the decay is only geometrical. The evidence of "geometrical damping" is also clear when Im $k = 0.042$ when one compares the one-dimensional result with the three-dimensional result.

To demonstrate the great sensitivity of the ion-acoustic field to the source specifications, we have repeated the derivation of Eq. (10) for the (somewhat more realistic) case of large ion acceleration in the dc sheath on the plasma side of the grid structure. Such sheaths have the effect of imparting a velocity v_0 to the ions, essentially normal to the grid plane, of magnitude much larger than the ion thermal speed. This simplification assumes the sheath thickness to be large compared with the spacing between grid wires (or, for a plasma in magnetic field, for the ion gyroradius to be small compared with the sheath size) so that the sheath acceleration is the same for all ions and is in the z direction. The theoretical approach must be modified so as to allow for large spatial changes in the static equilibrium ion distribution function in the region of the sheaths and grids. The complete derivation is given in Appendix B. The result is

$$\phi(r, z, \omega) = \frac{2E_0 a}{\pi}\frac{v_0}{\omega}\sin^2\left(\frac{\omega L}{2v_0}\right)\left(\frac{D_e(k_0)}{k_0^2(\partial D/\partial k)_{k_0}}\right)$$

$$\cdot\int_0^\infty dk_\perp\, J_1(k_\perp a)J_0(k_\perp r)\exp\left[-iz(k_0^2 - k_\perp^2)^{1/2}\right]. \quad (12)$$

The integral in Eq. (12) is identical to that in Eq. (10). Hence, E_z or J_z is proportional to the partial derivative with respect to z of Eq. (12). The noteworthy difference between the inclusion of the dc sheaths and no sheaths is that the Fresnel-like interference is not as pronounced in the former case.

What is clear from the examples given is that, in the weak damping limit, monotone decaying signals are only found in the far field (i.e., $z > 12.5$ cm for $\lambda = 0.7$ cm and $a = 2.25$ cm). In the near field, the complicated interference pattern is a sensitive function of source details. These features would tend to make inference of an accurate damping length from experimental data quite difficult. For strong damping, single-particle free-streaming motion of noninteracting particles is the dominant response. For small z the ballistic ions dominate whereas for large z the free-streaming electrons give the major plasma response. However, unlike Gould's model, the present boundary conditions do not allow perturbations of the electrons. Hence, the ion contribution dominates for a larger range of z for our chosen boundary conditions. This point is clarified in Appendix A. This fact should help to simplify interpretation of some nonlinear experiments, since complicated plasma shielding effects may, in fact, not enter.

IV. EXPERIMENTAL RESULTS

As discussed in Sec. II all data presented in this paper were taken under the following conditions:

$$n_i \simeq n_e = 5 \times 10^8\ \text{cm}^{-3}, \quad \omega_{pi}/2\pi = 740\ \text{kHz},$$

$$T_e = 0.80\ \text{eV}, \quad \lambda_D = 3 \times 10^{-2}\ \text{cm},$$

$$p_{\text{argon}} = 3\text{–}4\ \text{mTorr}.$$

The three-grid or four-grid transmitting electrode discussed above provided sufficient shielding of any direct-coupled signal to allow interferometric measurements to be made, as shown schematically in Fig. 1. Raw data are shown in Figs. 7 and 8. Figure 7 shows the response for 10 different values of ω/ω_{pi} ranging from 0.27 to 2.30 and collected ion current is plotted in relative units as a function of electrode separation. In Fig. 8 the data were taken at a lower background pressure.

Careful perusal of the data shown in Fig. 7 reveals several general features: (a) The signals have a well-defined periodicity for $\omega/\omega_{pi} < 0.812$; (b) the aperiodicity for $\omega/\omega_{pi} \geq 0.812$ would appear to result from mixing of at least two spatially periodic disturbances, both strongly decaying; (c) the signal modulus is not, in general, a monotone decaying function of receiver position, for $\omega/\omega_{pi} < 1$; in fact,

the data shows a region where signal magnitude increases with increasing receiver position, and (d) signal propagation for $\omega/\omega_{pi} > 1$ is extremely weak, with an attenuation length of the order of one spatial phase cycle.

The well-defined spatial periodicity at lower frequencies permits approximate determination of

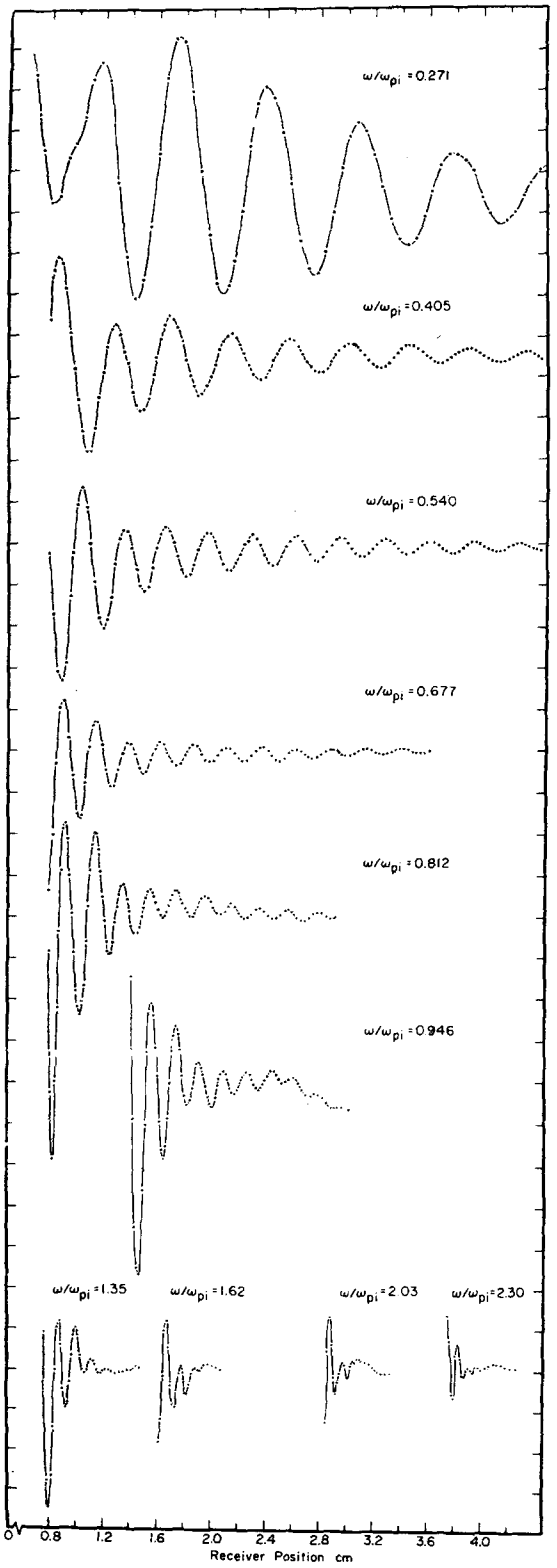

FIG. 7. Interferometer measurements of received ion current vs z at a background pressure of 4 mTorr.

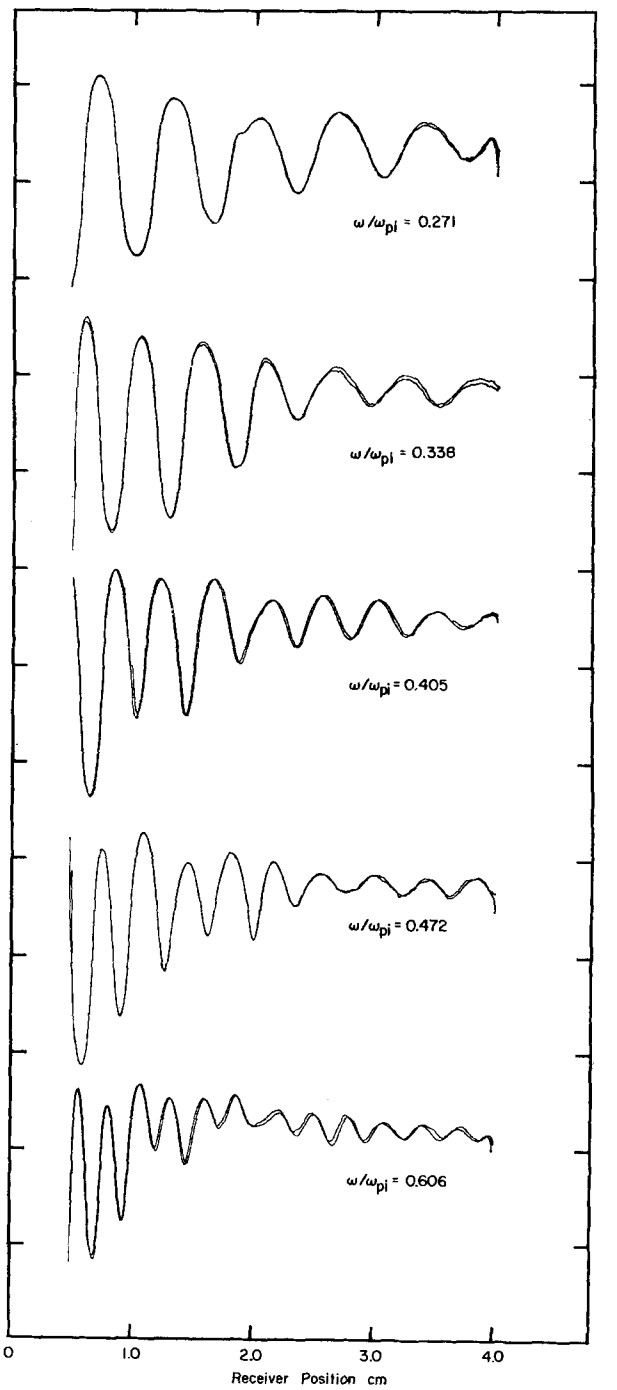

FIG. 8. Interferometer measurements of received ion current vs z at a background pressure of 3 mTorr. Notice a more pronounced Fresnel-like interference pattern.

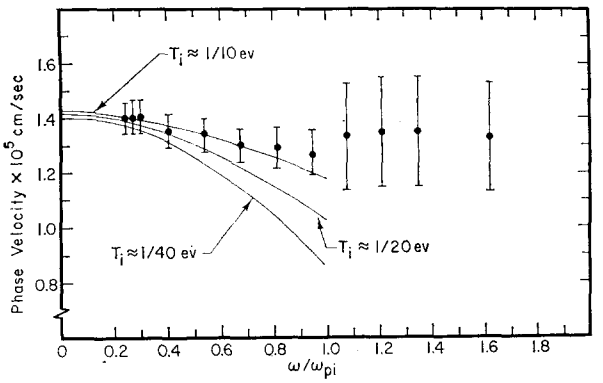

FIG. 9. Plot showing experimental points and theoretical curves of phase velocity versus ω/ω_{pi}. As $\omega/\omega_{pi} \rightarrow 0$, the phase velocity approaches the ion-acoustic value $[k(T_e + 3T_i)/M]^{1/2}$.

effective phase velocity. Figure 9 shows these determinations. Within experimental error, little, if any, dispersion is observable. Solid curves in Fig. 9 show the phase velocity $\omega/\mathrm{Re}\ k$ predicted for the one-dimensional collisionless theory, i.e., from the principal root of $D(\omega, k) = 0$, for $T_e = 0.80$ eV. Since the ion temperature T_i was not measured in these experiments, it is not possible to discuss the comparison between experiment and theory in detail. It may not be too surprising that the 20% theoretical dispersion for T_i equal to twice room temperature (0.05 eV) was not identified experimentally in view of the expected departures from plane wave propagation discussed above.

In Sec. III we showed that if $k_i \geq 1.076\ \mathrm{cm}^{-1}$, its value could be determined to a fair degree of accuracy if we assumed that the one-dimensional results were applicable. This value of k_i corresponds approximately to the collisional damping in argon at a background pressure of 4 mTorr. Hence, the data shown in Fig. 7 were fitted to a simple exponential decay. The resulting inferred values of k_i are shown in Fig. 10 as a function of normalized frequency ω/ω_{pi}. For $\omega/\omega_{pi} < 0.5$, the decrease in k_i/k_r is because of ion–atom collisions ν_{ia}. In fact, $k_i = \nu_{ia}/(\omega k_r)$ if ion–atom collisions are the only decay mechanism. This is shown by the solid curve in Fig. 10. Also shown by solid lines are the Landau damping for three different values of T_i. The dashed lines are the algebraic sum of the Landau and collisional damping. For $\omega/\omega_{pi} > 0.7$, Landau damping is no longer negligible. In fact at $\omega = 1.35\ \omega_{pi}$, the decay is almost completely due to Landau damping. The results in Fig. 10 suggest that T_i lies between 1/40 eV (room temperature) and 1/20 eV.

The data presented in Fig. 8, taken at a lower background pressure (3 mTorr), show a more pronounced Fresnel-like interference. The interference pattern has two dominant features: it becomes more pronounced with increasing distance from the source and with increasing ω; the number of Fresnel zones increases with frequency. These general features are consistent with the theory derived in Sec. III. In fact, in Fig. 11 the modulus of the current inferred from the data is compared to the theoretical result (including sheaths). In the numerical calculations of $|j_z(z)|$, k_i is taken to be $0.807\ \mathrm{cm}^{-1}$ which is attributed to collisional damping at a background pressure of 3 mTorr. The experimental and theoretical rates of decay compare favorably. In fact, for frequencies of 300, 350, and 450 kHz the experimental points are in very close agreement with the corresponding theoretical curves. This is remarkable considering that the Fresnel pattern is very sensitive to a precise knowledge of the ion-acoustic wavelength, which is dependent on $(T_e)^{1/2}$ (known to within 10%) as measured by the Langmuir probe. The great sensitivity of the Fresnel pattern to wavelength is apparent if one compares the theoretical curves of 300 and 350 kHz in Fig. 11. The vertical error bars are a

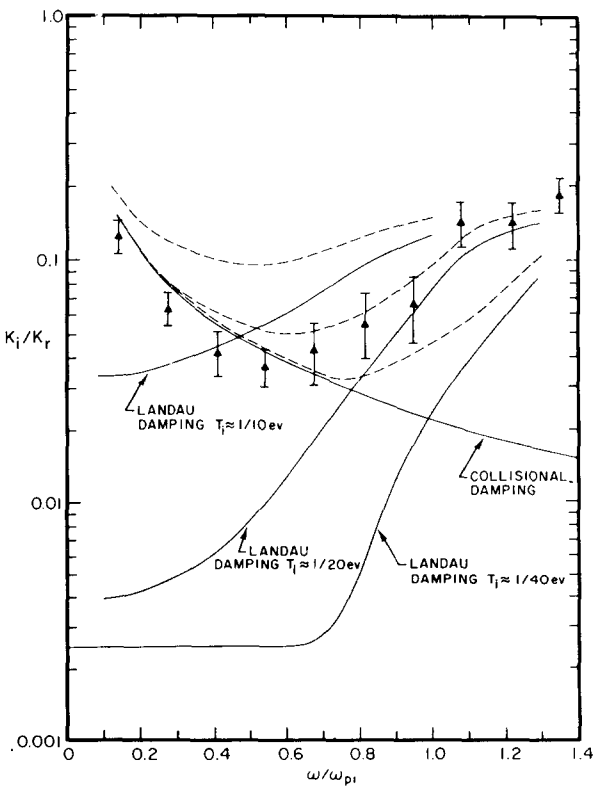

FIG. 10. Plot showing k_i/k_r vs ω/ω_{pi}. The points are inferred from data such as in Fig. 7. The collisional damping curve corresponds to an argon background pressure of 4 mTorr. The dashed curves are the algebraic sum of the collisional damping and Landau damping for various values of T_i.

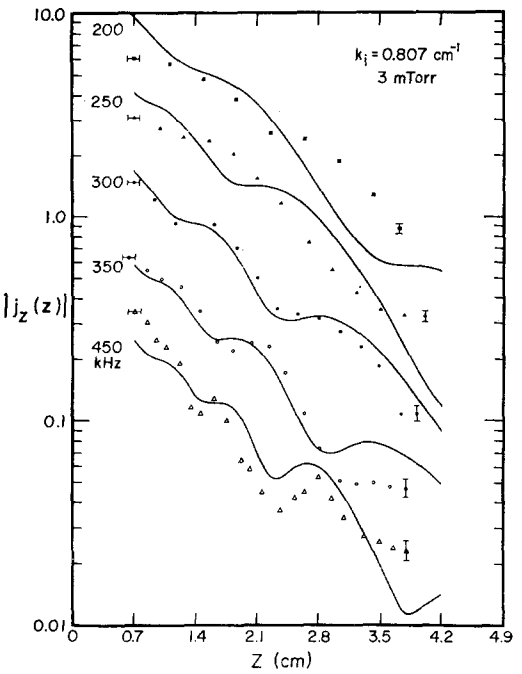

FIG. 11. A semilog plot showing $|j(z, r = 0)|$ vs z. The solid lines are theoretical curves of the received current density versus z. The experimental points are inferred from the data shown in Fig. 8. $k_i = 0.807$ cm^{-1} corresponds to collisional damping at a pressure of 3 mTorr.

result of noise. As the wave decays by an order of magnitude, these error bars will be 0.1 of the indicated size for the far left experimental points. The horizontal error bars are due to lack of knowledge of the precise distance between the receiver and source. In spite of the complications introduced by the source and three-dimensional motion of the particles we have essentially verified the linear dispersion relation for ion-acoustic waves. Landau damping has been observed as $\omega \to \omega_{pi}$ and the theoretically predicted cutoff at ω_{pi} has been verified. Three-dimensional effects, i.e., Fresnel-like interference has been clearly identified.

ACKNOWLEDGMENT

This work was supported in part by the National Science Foundation and in part by the Atomic Energy Commission.

APPENDIX A. DERIVATION OF EQ. (10) AND THE ELECTRON BALLISTIC CONTRIBUTION

The spatial response of the plasma is given by

$$\phi(r, z, \omega) = \frac{1}{(2\pi)^3} \int_0^\infty dk_\perp\, k_\perp \int_0^{2\pi} d\theta \exp(ik_\perp r \cos\theta) \cdot \int_{-\infty}^{+\infty} dk_z \exp(ik_z z)\phi(\mathbf{k}, \omega). \quad \text{(A1)}$$

Using Eq. (8) in Sec. III, Eq. (A1) becomes

$$\phi(r, z, \omega) = \frac{2E_0 a}{\pi} \int_0^\infty dk_\perp \int_{-\infty}^{+\infty} dk_z \frac{1}{k_z} \sin^2\left(\frac{k_z L}{2}\right) J_1(k_\perp a) \cdot J_0(k_\perp r)\left(\frac{D_e(k, \omega)}{D(k, \omega)}\right) \exp(-ik_z z). \quad \text{(A2)}$$

Now $k^2 = k_z^2 + k_\perp^2$ and $kdk = k_z dk_z$ taking $k_\perp$ fixed in performing the k_z integral. Making the above substitutions and replacing $\sin^2(k_z L/2)$ by $(k_z^2 L^2/4)$, Eq. (A2) can be written as

$$\phi(r, z, \omega) = \frac{E_0 a}{2\pi} \int_0^\infty dk_\perp \int_{-\infty}^{+\infty} dk \frac{kL^2}{(k^2 - k_\perp^2)^{1/2}} \cdot J_1(k_\perp a) J_0(k_\perp r)\left(\frac{D_e(k, \omega)}{D(k, \omega)}\right) \exp[-iz(k^2 - k_\perp^2)^{1/2}]. \quad \text{(A3)}$$

The functions $D_e(k, \omega)$ and $D(k, \omega)$ have branch cuts along the real k axis. Hence, we split the integration into positive k and negative k. Let D_1 be defined such that the contour in the v plane runs above the singularity and D_2 such that the contour runs below the singularity. If we neglect contributions that decay in a Debye length, Eq. (A3) reduces to

$$\phi(r, z, \omega) = \frac{E_0 a}{2\pi} \int_0^\infty dk_\perp \int_0^\infty dk \frac{kL^2}{(k^2 - k_\perp^2)^{1/2}} \cdot J_1(k_\perp a) J_0(k_\perp r) \exp[-iz(k^2 - k_\perp^2)^{1/2}] \cdot\left(\frac{D_{e1}(k, \omega)}{D_1(k, \omega)} - \frac{D_{e2}(k, \omega)}{D_2(k, \omega)}\right). \quad \text{(A4)}$$

Let us consider the portion of the intergrand represented by $[(D_{e1}/D_1) - (D_{e2}/D_2)]$ more closely. We find for a Maxwellian velocity distribution

$$D_1 D_2\left(\frac{D_{e1}}{D_1} - \frac{D_{e2}}{D_2}\right) = -i\left[1 + \frac{\omega_{pe}^2}{k^2 v_e^2} \operatorname{Re} Z'\left(\frac{\omega}{kv_e}\right)\right] \cdot \operatorname{Im}\left[\frac{\omega_{pi}^2}{k^2 v_i^2} Z'\left(\frac{\omega}{kv_i}\right)\right] + i \operatorname{Re}\left[\frac{\omega_{pi}^2}{k^2 v_i^2} Z'\left(\frac{\omega}{kv_i}\right)\right] \cdot \operatorname{Im} \frac{\omega_{pe}^2}{k^2 v_e^2} Z'\left(\frac{\omega}{kv_e}\right).$$

The factors

$$\operatorname{Im}[(\omega_{pi}^2/k^2 v_i^2) Z'(\omega/kv_i)]$$

and

$$\operatorname{Im}[(\omega_{pe}^2/k^2 v_e^2) Z'(\omega/kv_e)]$$

together with the exponent $\exp[-iz(k^2 - k_\perp^2)^{1/2}]$ give rise to saddle points k_{si} and k_{se}, respectively;

$$k_{si} = \left(\frac{2v_i}{\omega x}\right)^{1/3}\left(\frac{\omega}{v_i}\right) \exp\left(-\frac{i\pi}{6}\right),$$

$$k_{se} = \left(\frac{2v_e}{\omega x}\right)^{1/3}\left(\frac{\omega}{v_e}\right) \exp\left(-\frac{i\pi}{6}\right),$$

where we neglect the small effect of $k_\perp$ in the saddle point calculation. We may deform the contour running along the real k axis into the lower half-plane so as to run through the saddle points k_{si} and k_{se}. The contributions from these saddle points correspond to ion and electron ballistic contributions, respectively. The ion ballistic contribution arises because of ions that stream through the source electric field and the electric fields excited by the wave and source ballistic ions. The electron ballistic component arises because of electrons that stream through the electric field created by the wave and source ballistic ions. The dominant pole of D_1 lies in the lower half-plane whereas D_2 has a pole in the upper half-plane. In the weak damping limit $\omega < \omega_{pi}$ and $T_i \ll T_e$ we will pick up a contribution from the pole due to D_1. This will be the dominant response, and Eq. (A4) reduces to Eq. (10) in Sec. III.

In the heavy damping limit, when $\omega > \omega_{pi}$ or $T_e \approx T_i$ the dominant pole of D_1 recedes from the real axis. When k_i/k_r for this pole is about $(3)^{-1/2}$ or greater, the contribution from the saddle points k_{se} and k_{si} will be the dominant contribution. Hence in this limit, the ballistic contribution dominates.

Returning to the weak damping limit, because of the relatively long scale length of the electron ballistic contribution, we will expect it to dominate at large distances from the source. For simplicity, we will estimate this distance for a one-dimensional problem. When $\omega \ll \omega_{pi}$ and $T_i \ll T_e$, the electric field associated with the ion-acoustic wave is given by $E_{1\omega}(x)$

$$E_{1\omega}(x) \approx -iE_0L^2k_0^2 \exp(ik_0x). \tag{A5}$$

The electron ballistic contribution is given by[12] $E_{fse}(x)$

$$E_{fse}(x) \approx -i2\sqrt{2}\,E_0L^2\frac{\omega_{pi}}{\omega_{pe}}\frac{\omega^2}{v_e^2} \cdot\exp\left[\frac{3}{2}\left(\frac{\omega x}{v_e}\right)^{2/3}(i\sqrt{3}-1)\right]. \tag{A6}$$

Taking the ratios (A4) and (A5) we find

$$\left|\frac{E_{fse}(x)}{E_1(x)}\right| \approx \left(\frac{m}{M}\right)^2 \exp\left(-\frac{k_i}{k_r(M/m)^{1/2}}\right). \tag{A7}$$

In a weakly ionized plasma at a background of 2–4 mTorr k_i/k_r is slightly less than 0.1. Under these conditions the electron free-streaming contribution will begin to dominate for $\omega x/v_e \approx 1$ or $x \approx (M/m)(\lambda/2\pi)$. Hence, when $\omega/\omega_{pi} \ll 1$ and $T_i/T_e \ll 1$ the ion-acoustic wave dominates for several tens of wavelengths.

The experiment was performed under conditions such that the multiple grid transducer was floating. The plasma floating potential is given by[22]

$$\phi_f \approx \frac{KT_e}{2}\ln\frac{M}{m}.$$

This potential allows the high-energy electrons to pass through the multigrid transducer. The perturbed distribution function for these high-energy electrons is given by[12]

$$f_e(v > v_f, t, x \approx 0) = -\frac{eE_0}{m}\frac{\partial F_e}{\partial v} \cdot\left(\int_{t-L/v}^{t} dt' \sin\omega t' - \int_{L}^{L+t/v} dt' \sin\omega t'\right)\theta(v - v_f),$$

where θ is the unit step function, and $v_f = (2e\phi_f/m)^{1/2}$;

$$f_e(x > 0) = \frac{4eE_0}{m_e\omega}\frac{\partial F_e}{\partial v}\,\theta(v - v_f)\sin^2\frac{\omega L}{2v}\cos\omega\left(t - \frac{x}{v}\right).$$

The perturbed current density is given by

$$j_{fse}(x > 0) = -e\int f_e(x > 0)v\,dv$$

$$= \frac{e^2E_0}{\omega M_e}\,\mathrm{Re}\int_{v_f}^{\infty} dv\,v\frac{\partial F_e}{\partial v}\sin^2\left(\frac{\omega L}{2v}\right)\exp\left[i\omega\left(t - \frac{x}{v}\right)\right].$$

For $\omega x/v_e \ll 1$

$$j_{fse}(x > 0) \approx \frac{2\omega_{pe}^2}{4\pi}\frac{E_0\omega L^2}{\pi^{1/2}v_fv_e}\exp\left(-\frac{v_f^2}{v_e^2}\right) \approx \frac{\omega_{pe}^2}{2\pi}\frac{E_0\omega L^2}{\pi^{1/2}v_fv_e}\left(\frac{m}{M}\right)^{1/2}.$$

Now the plasma shielding of this current is given by $1/D \approx -\omega^2/\omega_{pe}^2$. Comparing this contribution to the free-streaming electron contribution arising from electrons moving in the source ballistic ion field and ion-acoustic wave field we find it is larger by roughly a factor $(M/m)^{1/2}$. However, this contribution will also be unimportant for the present experiment. (If our grids were transparent to both electrons and ions, the electron contribution would be larger than E_{fse} by a factor of M/m.)

The reduction of an electron signal, which might completely mask the ion-acoustic behavior at a moderate distance from the source, is encouraging from the point of view of an experimenter attempting to stimulate the ion-acoustic response. Since an immersed grid is almost always strongly biased so as to exclude electrons (and thus not draw current from a plasma), it would seem that any interpretation[6] depending upon a large free-streaming electron

component would necessarily have to include some explanation as to how statically excluded electrons are modulated near a source grid.[23]

APPENDIX B. FREE-STREAMING CHARGE PERTURBATION FROM NEGATIVELY BIASED GRIDS[24]

For strong negative bias on the perturbing grid structure, positive ions receive large dc axial acceleration in the sheaths surrounding the grids, and thus move through the intergrid space with uniform axial velocity. At exit, the sheath decelerates the ions as they re-enter the plasma.

We first solve, by trajectory integration, for the ion velocity distribution at the source. Here, the self-consistent electric field can be neglected. Thus,

$$f_i(\mathbf{r}, z = 0, \mathbf{v}, t) = \frac{e}{M}\int_{-\infty}^{t} dt' \exp(-i\omega t')\mathbf{E}_a(t', \mathbf{r}')\cdot\nabla_v F_i(\mathbf{v}, t', r'), \tag{B1}$$

where the ion trajectory is from far behind the grid, through the accelerating sheath, through the alternating intergrid field $\mathbf{E}_0(r, t)$ and through the decelerating sheath. We note that $\nabla_v F_i(\mathbf{v}, \mathbf{r}, t) = M\mathbf{v}\ \partial F_i(v)/\partial\epsilon$ where ϵ is the energy, and that $\partial F(v)/\partial\epsilon$ is a constant of the motion to lowest order in a perturbation expansion. Thus,

$$f_i(r, z = 0, \mathbf{v}, t) = e\frac{\partial F_i(v)}{\partial\epsilon}\int_{-\infty}^{t} dt' \exp(-i\omega t')\mathbf{v}'\cdot\mathbf{E}_a(\mathbf{r}', t'). \tag{B2}$$

But $e\mathbf{v}\cdot\mathbf{E}_0$ is the power delivered from the fields to an ion, i.e., $-e\ \partial\phi_0(\mathbf{r}', t')/\partial t'$, since in the intergrid space $\mathbf{v}' = \mathbf{v}_0$ is in the z direction and thus parallel to $\mathbf{E}_0$. For the grid fields given by $\phi_0(r, z) = \phi_0(r)(1 - |z|/L)$, where $\phi_0(r) = \phi_0$ for $0 < r < a$, $-L < z < L$; and $\phi_0(r) = 0$, otherwise, we then have

$$f_i(r, z \simeq 0, \mathbf{v}, t) = e\frac{\partial F_i(v)}{\partial\epsilon}\phi_0(r)\frac{v_0}{L}\cdot\left(\int_{-L/v_0}^{0} dt' \exp(-i\omega t') - \int_{0}^{L/v_0} dt' \exp(-i\omega t')\right);$$

$$f_i(r, z \simeq 0, \mathbf{v}, t) = \frac{i4e}{\omega}\frac{\partial F_i(v)}{\partial\epsilon}\phi_0(r)\frac{v_0}{L}\sin^2\left(\frac{\omega L}{2v_0}\right). \tag{B3}$$

This distribution free-streams along straight-line trajectories into the half-space $z > 0$. Thus,

$$f_i(r, z, t, \mathbf{v}) = f_i(r, 0, t, \mathbf{v})H\left[a^2 - \left(\mathbf{r} - \mathbf{v}\frac{z}{v_z}\right)^2\right]H(z),$$

where $H(\xi) = 1$ for $\xi \geq 0$ and $H(\xi) = 0$ for $\xi < 0$. The Fourier transformed function is

$$f_i(\mathbf{k}) = f_i(r, 0, t, \mathbf{v})\cdot\int d^3r \exp\left\{-i\left[\mathbf{k}\cdot\mathbf{r} - \omega\left(t - \frac{z}{v_z}\right)\right]\right\}H\cdot\left[a^2 - \left(\mathbf{r} - \mathbf{v}\frac{z}{v_z}\right)^2\right]H(z).$$

We change variables, with $\mathbf{r} - \mathbf{v}(z/v_z) = \mathbf{r}'$ and $|\mathbf{r}'| = \rho$. Thus,

$$f(\mathbf{k}) = f_i(r, 0, t, \mathbf{v})\int d^3r' \exp\left[-i\mathbf{k}_\perp\cdot\left(\mathbf{r}'_\perp + \mathbf{v}\frac{z}{v_z}\right)\right]\cdot\exp(-ik_z z)\exp\left[i\omega\left(t - \frac{\rho}{v_z}\right)\right]H(a^2 - \rho^2)H(z)$$

or

$$f(\mathbf{k}) = f_i(r, 0, t, \mathbf{v})\int_0^\infty dz\int_0^a d\rho\rho\int_0^{2\pi} d\phi\cdot\exp(-ik_\perp\rho\cos\phi)\exp\left(\frac{iz(\mathbf{k}_\perp\cdot\mathbf{v} + k_z v_z - \omega)}{v_z}\right) = f_i(r, 0, t, \mathbf{v})\frac{2\pi a}{k_\perp}J_\perp(k_\perp a)\frac{v_z}{i(\mathbf{k}\cdot\mathbf{v} - \omega)}, \tag{B4}$$

so that

$$\rho_{fs}(\mathbf{k}) = e\int d^3v\, f_i(\mathbf{v}, \mathbf{k}) = \frac{8\pi e^2 E_0}{M}\frac{a}{k_\perp}J_\perp(k_\perp a)\frac{v_0}{\omega}\sin^2\left(\frac{\omega L}{2v_0}\right)\int d^3v\frac{\hat{\mathbf{e}}_z\cdot\nabla_v F_i(v)}{\mathbf{k}\cdot\mathbf{v} - \omega} \tag{B5}$$

since $v_z\ \partial F_i(v)/\partial\epsilon = -\hat{\mathbf{e}}_z\cdot\nabla_v F_i(v)$, and with $E_0 = \phi_0/L$. The velocity integral is

$$\int d^3v\frac{\hat{\mathbf{e}}_z\cdot\nabla_v F_i(v)}{\mathbf{k}\cdot\mathbf{v} - \omega} = \frac{M}{4\pi e^2}k_z[D_e(k, \omega) - D(k, \omega)],$$

and the ion-acoustic charge perturbation follows as

$$\rho(\mathbf{r}) = \left(\frac{1}{2\pi}\right)^3\int d^3k \exp(i\mathbf{k}\cdot\mathbf{r})\frac{\rho_{fs}(\mathbf{k})}{D(k)}.$$

We evaluate this integral as before, treating $D^{-1}(k)$ as a sharply peaked function of k (for weak damping). Suppressing the contribution differing from zero only in the intergrid space, one finds the results given in Eq. (13).

---

[1] R. W. Revans, Phys. Rev. **44**, 798 (1933); F. W. Crawford, Phys. Rev. Letters **6**, 663 (1961); P. F. Little, Nature **194**, 1137 (1962); F. W. Crawford and S. A. Self, in *Proceedings of the Sixth International Conference on Ionization Phenomena in Gases*, edited by T. Hubert and E. Crémien (Bureau des Editions, Centre d' Etudes Nucléaires de Saclay, Paris, 1964), Vol. 3, p. 129.

[2] A. Y. Wong, N. D'Angelo, and R. W. Motley, Phys. Rev. Letters **9**, 415 (1962); R. W. Motley and A. Y. Wong, in *Proceedings of the Sixth International Conference on Ionization Phenomena in Gases*, edited by T. Hubert and E. Crémien (Bureau des Editions Centre d' Etudes Nucléaires de Saclay, Paris, 1964), Vol. 3, p. 133.

[3] R. W. Gould, Phys. Rev. **136**, A991 (1964).
[4] A. Y. Wong, R. W. Motley, and N. D'Angelo, Phys. Rev. **133**, A436 (1964).
[5] B. D. Fried and R. W. Gould, Phys. Fluids **4**, 139 (1961).
[6] A. Y. Wong, Phys. Rev. Letters **14**, 252 (1965).
[7] H. Sato, H. Ikezi, N. Takahashi, and Y. Yamashita, Phys. Rev. **183**, 278 (1969).
[8] H. K. Andersen, N. D'Angelo, V. O. Jensen, P. Michelsen, and P. Nielsen, Phys. Fluids **11**, 1177 (1968).
[9] I. Alexeff and W. D. Jones, Phys. Rev. Letters **15**, 286 (1965); I. Alexeff, W. D. Jones, and D. Montgomery, Phys. Fluids **11**, 167 (1967).
[10] G. M. Sessler, Phys. Rev. Letters **17**, 243 (1966).
[11] G. M. Sessler and G. A. Pearson, Phys. Rev. **162**, 108 (1967).
[12] J. L. Hirshfield and J. H. Jacob, Phys. Fluids **11**, 411 (1958).
[13] H. J. Doucet and D. Gresillon, Phys. Letters **28A**, 257 (1968); N. Sato, H. Ikezi, Y. Yamashita, and N. Takahashi, Phys. Rev. Letters **20**, 837 (1968).
[14] H. Ikezi and N. Takahashi, Phys. Rev. Letters **20**, 140 (1968); D. R. Baker, N. R. Ahern, and A. Y. Wong, Phys. Rev. Letters **20**, 318 (1968).
[15] The Debye length used in these estimates was that of the body of the plasma. In the intergrid spacing, the value is about 10 times larger due to the density decrease accompanying ion acceleration in the ~6 V dc sheaths.
[16] While the details of this grid structure may appear to be rather specialized, its design was the simplest of any considered which would be capable of quantitative understanding. Other experimenters have launched spatial disturbances using wire probes and single grids. The former provides a strongly nonuniform excitation and is ill-suited for calculation of the ion perturbations induced, since the rf and dc electric fields near the elctrode are not known. The latter suffers from the same difficulty, but additionally introduces larger direct capacitive coupling between the transmitting and receiving grids, which can mask the propagating waves.
[17] E. G. Broadbent, Proc. Roy. Soc. (London) **A311**, 211 (1969).
[18] J. H. Jacob and J. L. Hirshfield, in *Proceedings of the International Conference on Physics of Quiescent Plasmas*, Paris (Ecole Polytechnique, Paris, 1969), Vol. I, p. 93.
[19] It should be noted that Gould[3] was able to treat a symmetric source because he neglected the reflection of the electrons by the static sheaths.
[20] B. D. Fried and S. D. Conte, *The Plasma Dispersion Function* (Academic, New York, 1961).
[21] I. M. Ryshik and I. S. Gradstein, *Tables of Series, Products and Integrals* (VEB Deutscher Verlag der Wissenschaften, Berlin, 1957), p. 237.
[22] F. F. Chen, in *Plasma Diagnostic Techniques*, edited by R. H. Huddlestone and S. L. Leonard (Academic, New York, 1965), p. 178.
[23] For a grid whose intermesh dimension exceeds a Debye length, these considerations fail, but the source function is then strongly inhomogeneous in the grid plane.
[24] This derivation is due largely to I. B. Bernstein.

THE PHYSICS OF FLUIDS VOLUME 14, NUMBER 3 MARCH 1971

Symmetry Considerations for Grid-Launched Ion-Acoustic Waves

I. B. Bernstein, J. L. Hirshfield, and J. H. Jacob
Mason Laboratory, Yale University, New Haven, Connecticut 06520
(Received 9 March 1970)

Immersion of a fine-mesh grid (or set of parallel grids) into a plasma is widely used to stimulate ion-acoustic waves. The grid structure is usually biased so as to reflect electrons and transmit ions. The effect upon the ions due to applied rf fields in the grid region is to provide some combination of velocity and density modulation. The associated applied electric field perturbations will possess a combination of odd and even spatially symmetric parts, about the plane of symmetry of the grid system. The steady-state solution of the governing differential equation in the ion-acoustic limit is shown to depend critically upon this source symmetry, and to reduce to the usual solution only for the case of odd symmetry. Experiments designed to test these symmetry predictions have been carried out using an apparatus described previously, except that a four-grid transmitter has been substituted for the three-grid one. The outer two grids are grounded and the inner two grids can be driven either in phase (odd E-field symmetry), or 180° out of phase (even E-field symmetry). For odd symmetry, the observed spatial disturbance is similar to that reported previously with clear evidence of Fresnel interference. For even symmetry, wavelike signals are not observed near the grids, indicating a strong decrease in coupling between the free-streaming source ions and an ion-acoustic wave.

I. INTRODUCTION

This paper is part of a series devoted to examination of the excitation of linearized low-frequency electrostatic disturbances in uniform plasmas without static magnetic fields. Particular emphasis has been on the difficulties in interpretation of the spatial decay observed experimentally when a steady-state signal is launched in plasma by driving an immersed electrode from an external generator. Thus, one calculation[1] has shown that the free-streaming drifts of ions or electrons which have been perturbed by a planar source gives rise to a spatial decay even in the absence of mutual interaction between the particles. The heavy damping limit for an ion-acoustic wave is dominated by this ballistic contribution. The ballistic contribution was first evaluated by Landau in the half-space electron plasma wave problem,[2] but not clearly identified as such. A rough criterion was given by us that observed decays should have an imaginary-to-real wavenumber ratio k_i/k_r somewhat less than 0.4 in order for collective effects to be clearly dominant in the decay.